Energy Spectrum of the Electrons in Graphene

Bachelor Thesis

at the Institute for Theoretical Physics,
Albert Einstein Center for Fundamental Physics,
University of Bern
by

Carla Gross

July 2011

Supervisor:

Prof. Dr. Uwe-Jens Wiese

Institute for Theoretical Physics, University of Bern

Abstract

In this bachelor thesis we investigate the energy spectrum of the quasi-free electrons in graphene. This is done in two ways; by diagonalizing the Hamiltonian of the Hubbard model, but also by deriving an effective low-energy field theory. If only low-energy excitations are considered, one can see that these electrons obey a linear dispersion relation. At the end of this thesis, when we calculate the energy of the electrons in an external magnetic field, we find that the magnetic field quantizes the energy values.

Contents

1 Introduction

Carbon is a very interesting and significant element for mankind; it is fundamental to the existence of life on Earth. A whole branch of chemistry, organic chemistry, is dedicated to it. The carbon atom has four valence electrons which can bind to an electron of another atom. As was pointed out by A. Geim [1], its flexible bonds cause it to occur in many differently structured forms and the dimensions of these forms result in a lot of different properties.

Graphite is one of these various carbon compounds. It consists of many layers, stacked upon each other, bound by the weak van der Waals force. Each layer is made of carbon atoms arranged on a honeycomb lattice which is illustrated in figure 1. Graphite has been known for a long time, especially since the invention of the pencil in 1564. But a lot of time passed, until graphene, a single atomic layer of graphite, was isolated by K. Novoselov in 2004. One of the reasons it had taken so long, was according to A. Geim [2], the fact that no scientist expected graphene to exist. So, there was great astonishment in the scientific community when K. Novoselov accomplished the isolation of a single layer by a simple scotch-tape technique. Because it can be attained so easily, graphene experienced a break-through in condensed matter physics in the last 6 years. Since 2005, when A. Geim and K. Novoselov published their work, thousands of papers have been written on graphene and it seems to be very promising in many applications of technology, for example, in computer electronics or in ultrahigh-frequency transistors. Therefore, in 2010, A. Geim and K. Novoselov were awarded the Nobel Prize in physics.

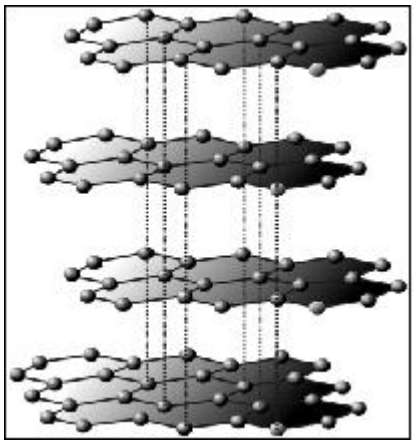

Figure 1: Graphite consisting of single atomic layers called graphene. [3]

The "graphene boom" is not only due to its prospects, but also to its amazing properties. As A. Geim stated in [1], it is the thinnest and strongest material; its breaking strength is about $40\frac{N}{m}$. It is impermeable to gases, it shrinks with increasing temperature, it can be stretched by 20% and it has a thermal conductivity of about $5000\frac{W}{mK}$ at room-temperature. It has a high pliability, but also a high brittleness and there are many more astonishing properties. Its chemistry is yet to be explored although it has very interesting chemical features, consisting only of two surfaces.

On the other hand, there is an intense research going on about the electronic properties of graphene, as is described in [1]. Since it is a single atomic layer, it is very sensitive to the proximity of other materials, for example, attaching a superconducting material results in a supercurrent flow. The electrons in graphene can propagate up to a few micrometers without scattering. Their dispersion relation, which is calculated in this thesis, is linear, therefore the same as for ultrarelativistic particles. This means that the electrons in the honeycomb lattice behave like massless particles, the fastest ones moving with a Fermi velocity v_F, being a fraction of the speed of light. Such

particles are called Dirac fermions. Applying a magnetic field perpendicular to the graphene layer causes a quantization of the energy spectrum; the Landau levels, which are also a subject of this thesis. The anomalous half-integer quantum Hall effect is a result of these discrete energy levels. The fact that it can be observed in graphene at room temperature is remarkable.

This thesis is also about the electronic properties of graphene. The energy spectrum of the electrons is calculated in two different ways. At the end of the thesis the Landau-levels are computed but the half-integer quantum Hall effect is not discussed. For further information one can read [2]. The thesis is structured in the following way: in section 2, the honeycomb lattice is discussed, the reciprocal lattice is introduced, some properties of the first Brillouin zone are pointed out and the Fourier transformation on the lattice, which is a integration over the first Brillouin zone, is derived. In section 3, the Hubbard model is introduced. This model allows us to compute the energy dispersion relation of the electrons. The energy is computed for electrons which can hop from a lattice point to its nearest neighbours, but also for ones which move to next-to-nearest neighbours. Considering only low energies, the spectra have the form of Dirac cones. These low-energy electrons obey a linear dispersion relation like massless particles and they propagate with a Fermi velocity $v_F = \frac{a\sqrt{3}t}{2\hbar} \approx 9 \cdot 10^5 \frac{m}{s}$. An effective low-energy field theory for these electrons is derived in section 4. It results in a $2+1$ dimensional Dirac equation for particles with zero mass. In section 5, the energy of the electrons in a magnetic field is computed in both the Hubbard model and the effective theory. One will notice that the energy is quantized in the discrete Landau-levels. Finally, in section 6, my conclusions are presented.

2 Honeycomb Lattice

Graphene is made of carbon atoms, which are arranged on a honeycomb lattice. This structure is a result of the bonds between the atoms. Carbon has in total six electrons, four of them being valence electrons. In the groundstate, two electrons are in the $2s$-orbitals and the other two in the $2p$-orbitals. When one of the electrons in the $2s$-orbital gets excited to the $2p$-orbital, the remaining s-orbital and two of the p-orbitals mix to form the sp^2-hybrid orbital. This linear combination is called sp^2 hybridization [2]. Two sp^2-hybridized electrons of two different atoms create a σ-bond, which is a single covalent bond. All carbon atoms in graphene are bound to each other by three σ-bonds. They enclose an angle of 120°. Therefore these bonds cause the trigonal planar structure of graphene and also its robustness. The distance of two carbon atoms d is equal to 1.42 $\mathring{A}$ [2]. The sp^2-hybridized electrons cannot propagate in the lattice. The remaining p-orbital is perpendicular to the plane. Two overlapping p-orbitals results in a π-orbital, which is also called a π-band because the electrons are delocalized in it. They can move around, thus being the cause of the conducting properties of graphene.

2.1 Spatial lattice

The (spatial) honeycomb lattice of graphene is shown in figure 2. It is a non-Bravais bipartite lattice, which means that it consists of two interpenetrating sublattices (black and blank points), each of them forming a triangular Bravais lattice. A Bravais lattice is a, in our case, two-dimensional, infinite arrangement of points which is generated by a set of discrete translations [4]. To perform the discrete translation operation, two primitive vectors $\vec{a}_1$ and $\vec{a}_2$ are needed

$$\vec{a}_1 = \begin{pmatrix} 1 \\ 0 \end{pmatrix} a, \qquad \vec{a}_2 = \begin{pmatrix} \frac{1}{2} \\ \frac{\sqrt{3}}{2} \end{pmatrix} a. \tag{1}$$

Here, a denotes the distance between two neighbouring points of the same sublattice, and is related to the distance d of two carbon atoms by $a = \sqrt{3}d = 2.46\,\mathring{A}$. The origin of the coordinate system is placed in the center of a hexagon. Therefore, to describe the blank and black points, two translation vectors $\vec{v}_1$ and $\vec{v}_2$ are used

$$\vec{v}_1 = \begin{pmatrix} 0 \\ 1 \end{pmatrix} \frac{a}{\sqrt{3}} = -\frac{1}{3}\vec{a}_1 + \frac{2}{3}\vec{a}_2, \qquad \vec{v}_2 = \begin{pmatrix} 0 \\ -1 \end{pmatrix} \frac{a}{\sqrt{3}} = \frac{1}{3}\vec{a}_1 - \frac{2}{3}\vec{a}_2. \tag{2}$$

All the black points $\vec{x}_\bullet$ are defined by

$$\vec{x}_\bullet = n_1\vec{a}_1 + n_2\vec{a}_2 + \vec{v}_1, \qquad n_1, n_2 \in \mathbb{Z}, \tag{3}$$

and the blank ones $\vec{x}_\circ$ by

$$\vec{x}_\circ = n_1\vec{a}_1 + n_2\vec{a}_2 + \vec{v}_2, \qquad n_1, n_2 \in \mathbb{Z}. \tag{4}$$

2.2 Symmetries of the Lattice

In this subsection, the symmetries of the honeycomb lattice are discussed. One should pay attention to whether it is a symmetry of the honeycomb lattice, but also of each sublattice, or whether it is only a symmetry of the honeycomb lattice. The former means that each sublattice is invariant under the symmetry transformation and the latter results in a transposition of the two sublattices.

2.2.1 Translation Symmetry

Since each of the two sublattices is a Bravais lattice, it is invariant under a translation of the two primitive vectors $\vec{a}_1$ and $\vec{a}_2$.

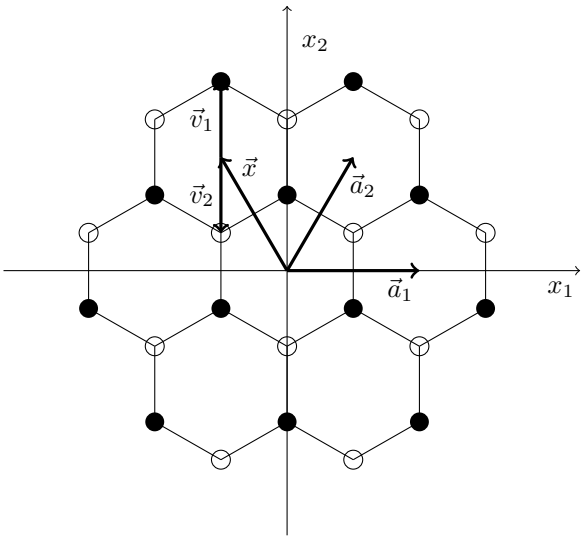

Figure 2: Honeycomb lattice with the primitive vectors $\vec{a}_1$ and $\vec{a}_2$.

2.2.2 Rotation Symmetry

A hexagon is invariant under a rotation of 60°. Thus the honeycomb lattice is too, but this rotation causes the two sublattice to interchange. Only a rotation by 120° is a symmetry of each sublattice.

2.2.3 Reflection Symmetry

The honeycomb lattice has six reflection axes. Three of them are parallel to the edges of a hexagon, and a reflection about these axes maps each sublattice onto itself. The other three axes are perpendicular to the edges of the hexagon, and they cause the sublattices to be mirrored onto each other.

2.3 Reciprocal Lattice

The reciprocal honeycomb lattice, which is illustrated in figure 3, is the set of all vectors $\vec{k}$ which obey the Laue condition [4]

$$\exp(i\vec{k} \cdot \vec{x}) = 1, \tag{5}$$

which is equal to

$$\vec{k} \cdot \vec{x} = 2\pi N, \qquad N \in \mathbb{Z}. \tag{6}$$

The reciprocal lattice is rotated by 30° in respect to the spatial lattice. Its primitive vectors $\vec{b}_1$ and $\vec{b}_2$ can be derived from

$$\vec{a}_i \cdot \vec{b}_j = \delta_{ij}, \tag{7}$$

$$\vec{b}_1 = \begin{pmatrix} \frac{\sqrt{3}}{2} \\ -\frac{1}{2} \end{pmatrix} b = \begin{pmatrix} \frac{\sqrt{3}}{2} \\ -\frac{1}{2} \end{pmatrix} \frac{4\pi}{\sqrt{3}a}, \qquad \vec{b}_2 = \begin{pmatrix} 0 \\ 1 \end{pmatrix} b = \begin{pmatrix} 0 \\ 1 \end{pmatrix} \frac{4\pi}{\sqrt{3}a}. \tag{8}$$

A vector in the reciprocal space can now be written as

$$\vec{k} = k_1\vec{b}_1 + k_2\vec{k}_2, \qquad k_1, k_2 \in \mathbb{Z}. \tag{9}$$

It is interesting to notice, that two electrons with the same spin can occupy the same site in the reciprocal lattice, when they each belong to a different sublattice [5]. Hence the indices $\circ$, $\bullet$ are two additional quantum numbers.

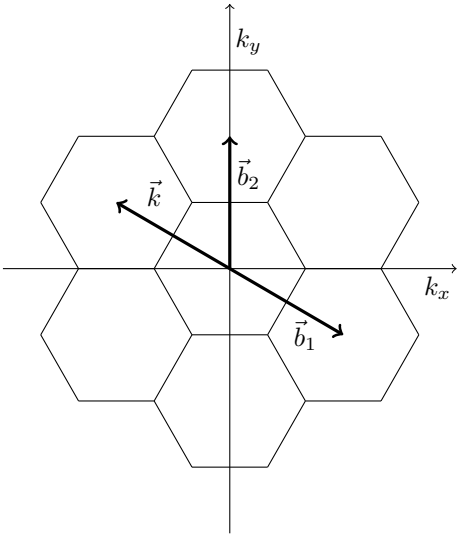

Figure 3: Reciprocal honeycomb lattice with the primitive vectors $\vec{b}_1$ and $\vec{b}_2$.

2.3.1 The First Brillouin Zone

The first Brillouin zone is a primitive cell in the reciprocal lattice. All the reciprocal vectors can be reduced to one lying in the first Brillouin zone, by a combination of the primitive vectors. The first Brillouin zone of a hexagonal lattice has a hexagonal form. To perform a Fourier transformation, we will need to integrate over the area of the first Brillouin zone, which is equal to $\frac{8\pi^2}{\sqrt{3}a^2} = 7.53\mathring{A}^2$. Integrating along the primitive vectors from $-\frac{1}{2}$ to $\frac{1}{2}$, creates a parallelogram. The area of the parallelogram is the same as the one of the first Brillouin zone, which is shown in figure 4. The six corners of the first Brillouin zone have the following coordinates:

$$\begin{pmatrix} \frac{4\pi}{3a} \\ 0 \end{pmatrix}, \quad \begin{pmatrix} -\frac{4\pi}{3a} \\ 0 \end{pmatrix}, \quad \begin{pmatrix} \frac{2\pi}{3a} \\ \frac{2\pi}{\sqrt{3}a} \end{pmatrix}, \quad \begin{pmatrix} -\frac{4\pi}{3a} \\ \frac{2\pi}{\sqrt{3}a} \end{pmatrix}, \quad \begin{pmatrix} \frac{4\pi}{3a} \\ -\frac{2\pi}{\sqrt{3}a} \end{pmatrix} \quad \text{and} \quad \begin{pmatrix} -\frac{4\pi}{3a} \\ -\frac{2\pi}{\sqrt{3}a} \end{pmatrix}. \tag{10}$$

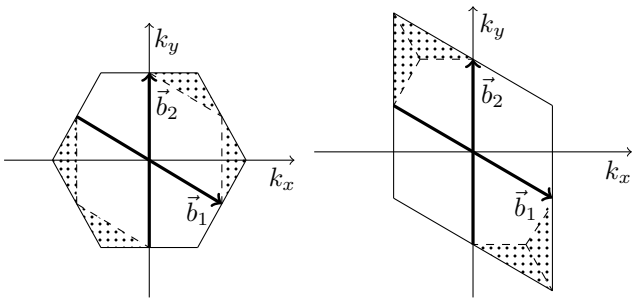

Figure 4: The hexagon to the left and the parallelogram to the right hand side are related by parallel transport.

2.4 Fourier Transformation

To switch between the spatial and the reciprocal lattice, one must perform a discrete Fourier transformation. The Fourier transformation has the following form

$$\tilde{f}(\vec{k}) = \sum_{\vec{x}} f_{\vec{x}} \exp(-i\vec{k} \cdot \vec{x}), \tag{11}$$

and its inverse Fourier transformation looks as follows

$$f_{\vec{x}} = \frac{\sqrt{3}a^2}{8\pi^2} \int_B d^2k\, \tilde{f}(\vec{k}) \exp(i\vec{k}\cdot\vec{x}). \tag{12}$$

Here B indicates the Brillouin zone. Knowing that the Fourier transformed Kronecker-δ is equal to one, we can derive its Fourier transformation, which is done below (13), and prove the above relations (11) and (12).

$$\begin{aligned}
\delta_{\vec{x},0} &= \delta_{n_1,0}\delta_{n_2,0} = \frac{\sqrt{3}a^2}{8\pi^2} \int_B d^2k \exp(i\vec{k}\cdot\vec{x}) = \int_{-\frac{1}{2}}^{\frac{1}{2}} dk_1 \int_{-\frac{1}{2}}^{\frac{1}{2}} dk_2 \exp(2\pi i(k_1 n_1 + k_2 n_2)) \\
&= \begin{cases} \int_{-\frac{1}{2}}^{\frac{1}{2}} dk_1 \int_{-\frac{1}{2}}^{\frac{1}{2}} dk_2 = 1 \qquad \text{for } i = j \\ \left(\frac{1}{2\pi i n_1}\right)\left(\frac{1}{2\pi i n_2}\right) \Big(\underbrace{\exp(i\pi n_1) - \exp(-i\pi n_1)}_{0}\Big) \Big(\underbrace{\exp(i\pi n_2) - \exp(-i\pi n_2)}_{0}\Big) = 0 \\ \qquad \text{for } i \neq j \end{cases}
\end{aligned} \tag{13}$$

In (13) we performed the substitution $k_x, k_y \to k_1, k_2$

$$k_x = \frac{2\pi}{a} k_2, \qquad k_y = \frac{4\pi}{\sqrt{3}a} k_1 - \frac{2\pi}{\sqrt{3}a} k_2. \tag{14}$$

The absolute value of the Jacobian determinant is $\frac{8\pi^2}{\sqrt{3}a^2}$, which is exactly the area of the Brillouin zone. Similarly the Dirac-δ is given by

$$\delta(\vec{k}) = \frac{\sqrt{3}a^2}{8\pi^2} \sum_{\vec{x}} \exp(-i\vec{k}\cdot\vec{x}). \tag{15}$$

3 Hubbard Model

The Hubbard model was first presented by Hubbard, Gutzwiler and Kanamori. It is a minimal model for spin $\frac{1}{2}$-particles hopping on a two dimensional lattice.

3.1 Electron Propagation

Each carbon atom in graphene has three neighbours, and is assumed to be pointlike. Three of the four electrons of a carbon atom are bound by a covalent σ-bond. The fourth electron can propagate through the lattice. It is delocalized in the π-band. Since every carbon atom contributes one electron to the π-band, it is half-filled. Thus the Hubbard model is analyzed at half-filling. The description of the hopping of the electrons is achieved through the creation operator $c^\dagger_{\vec{x},s}$, which creates an electron with spin s at the site $\vec{x}$, and the annihilation operator $c_{\vec{x},s}$, which eliminates an electron. The index s denotes the spin of the electron. The Pauli exclusion principle must be fulfilled. Hence a lattice site can either be empty, filled with one electron of spin up or down, or it can be occupied by two electrons of opposite spin, but never by two electrons of identical spin. Therefore the following anti-commutation rules apply to the operators

$$\{c_{\vec{x},s}, c_{\vec{x}',s'}\} = 0, \qquad \left\{c^\dagger_{\vec{x},s}, c^\dagger_{\vec{x}',s'}\right\} = 0, \qquad \left\{c^\dagger_{\vec{x},s}, c_{\vec{x}',s'}\right\} = \delta_{\vec{x},\vec{x}'}\delta_{s,s'}. \tag{16}$$

Applying the discrete Fourier transformation to these operators leads to

$$c^\dagger_s(\vec{k}) = \sum_{\vec{x}} c^\dagger_{\vec{x},s} \exp(i\vec{k}\cdot\vec{x}), \qquad c_s(\vec{k}) = \sum_{\vec{x}} c_{\vec{x},s} \exp(-i\vec{k}\cdot\vec{x}), \tag{17}$$

and its inverse Fourier transformation to

$$c^\dagger_{\vec{x},s} = \frac{\sqrt{3}a^2}{8\pi^2}\int_B d^2k\, c^\dagger_s(\vec{k}) \exp(-i\vec{k}\cdot\vec{x}), \qquad c_{\vec{x},s} = \frac{\sqrt{3}a^2}{8\pi^2}\int_B d^2k\, c_s(\vec{k}) \exp(i\vec{k}\cdot\vec{x}). \tag{18}$$

In this thesis, a Hubbard model, which describes the energy resulting from the hopping of all the pseudo-free electrons, is used. As already pointed out, the Hubbard Hamiltonian is considered at half-filling. One could also add more terms to the Hamiltonian, which for example account for the Coulomb repulsion of the electrons. However, in this work, only the following Hamiltonian is used for the calculations

$$\mathbb{H} = t \sum_{\langle\vec{x},\vec{y}\rangle,s} c^\dagger_{\vec{x},s} c_{\vec{y},s} + c^\dagger_{\vec{y},s} c_{\vec{x},s} \tag{19}$$

where t is the probability amplitude to tunnel between two neighbouring lattice sites, and $\langle\vec{x},\vec{y}\rangle$ is such a pair of neighbouring points. One should notice that this Hamiltonian only considers the electron hopping to nearest neighbours. For next-to-nearest neighbour hopping more terms must be added, which is done in section 3.4.

3.2 Symmetries of the Hubbard Model

In this section, the symmetries of the Hubbard Hamiltonian are pointed out, which are used later on to construct an effective theory. A symmetry of a system is an invariance of this system under a certain operation. Each continuous symmetry implies a conservation of a current, as stated by Noether's theorem. A symmetry of the Hamiltonian means that the energy is invariant under a particular change. The Hubbard Hamiltonian (19) has three discrete symmetries, which arise from the geometry of the lattice and three continuous symmetries. The following discussion is based on [5].

3.2.1 Discrete Symmetries

Not only the honeycomb lattice, but also the Hubbard Hamiltonian is invariant under the discrete symmetries: Translation, rotation and reflection (section 2.2). The Hamiltonian is symmetric under a translation along the two primitive vectors. Applying a unitary translation operator D on the annihilation operator yields

$$^{D}c_{\vec{x},s} = D^{\dagger}c_{\vec{x},s}D = c_{\vec{x}+\vec{a}_i,s}. \tag{20}$$

Now one can prove easily that the whole Hamiltonian (19) remains invariant; $[\mathbb{H}, D] = 0$. The Hamiltonian is also symmetric under a rotation by 60° although this results in an interchange of the two sublattices. The rotation operator O acts in the following way

$$^{O}c_{\vec{x},s} = O^{\dagger}c_{\vec{x},s}O = c_{O\vec{x},s}. \tag{21}$$

A point reflection at the lattice site $\vec{x}$ results in an interchange of the two sublattices too, but leaves the Hamiltonian invariant. This can be achieved through the reflection operator R

$$^{R}c_{\vec{x},s} = R^{\dagger}c_{\vec{x},s}R = c_{R\vec{x},s}. \tag{22}$$

3.2.2 $SU(2)_S$ Spin Symmetry

The Hubbard Hamiltonian has as $SU(2)_S$ spin symmetry. The $SU(2)_S$ group includes all (2×2) matrices which are unitary and have determinant 1. The corresponding operator V has the following form

$$V = \exp\left(i\vec{\eta}\cdot\vec{S}\right), \tag{23}$$

where $\vec{S}$ is the spin generator

$$\vec{S} = \sum_{\vec{x}} \vec{S}_{\vec{x}} = \sum_{\vec{x}} c^{\dagger}_{\vec{x}}\frac{\vec{\sigma}}{2}c_{\vec{x}}. \tag{24}$$

Here, $\vec{\sigma}$ are the Pauli matrices of eq.(53). By applying V on the annihilation operator

$$^{S}c_{\vec{x}} = V^{\dagger}c_{\vec{x}}V = \exp\left(i\vec{\eta}\cdot\frac{\vec{\sigma}}{2}\right)c_{\vec{x}}, \qquad \exp\left(i\vec{\eta}\cdot\frac{\vec{\sigma}}{2}\right) \in SU(2)_S, \tag{25}$$

one can show that the Hamiltonian is invariant, and that it commutes with the spin operator; $\left[\mathbb{H}, \vec{S}\right] = 0$, which implies that the total spin is conserved.

3.2.3 $U(1)_Q$ Charge Symmetry

The $U(1)_Q$ charge symmetry is an invariance under a phase transformation. The transformation achieved through the operator W leaves the Hubbard Hamiltonian invariant

$$W = \exp\left(i\omega Q\right), \tag{26}$$

where Q denotes the charge or the fermion number with respect to half-filling

$$Q = \sum_{\vec{x}} Q_{\vec{x}} = \sum_{\vec{x},s}\left(c^{\dagger}_{\vec{x},s}c_{\vec{x},s} - 1\right). \tag{27}$$

The invariance of the Hamiltonian can be proved taking the following equation into consideration

$$^{Q}c_{\vec{x}} = W^{\dagger}c_{\vec{x}}W = \exp\left(i\omega\right)c_{\vec{x}}, \qquad \exp\left(i\omega\right) \in U(1)_Q. \tag{28}$$

The $U(1)_Q$ charge symmetry implies a conservation of charge, or, equivalently, a conservation of the fermion number; $[\mathbb{H}, Q] = 0$.

3.2.4 $SU(2)_Q$ Pseudo-Spin Symmetry

Yang and Zhang proved that the $U(1)_Q$ charge symmetry of the Hubbard Hamiltonian can be extended to a non-Abelian $SU(2)_Q$ pseudo-spin symmetry [6]. The $U(1)_Q$ charge symmetry is a subgroup of the $SU(2)_Q$ symmetry, which is not discussed in detail here. This symmetry causes the symmetric energy values of electrons and holes, which are calculated in the next section. The symmetry breaks down when the Hamiltonian is modified to account for next-to-nearest neighbour hopping as in section 3.4.

3.3 Hopping to Nearest Neighbours

In this section, the energy values of the Hubbard Hamiltonian, which describes only nearest neighbour hopping are computed, which means that the Hamiltonian has to be diagonalized. In the case of graphene, there are two sublattices. Hence we must distinguish the c operators according to where they take effect. The Hamiltonian now takes the following form

$$\mathbb{H} = t \sum_{\langle \vec{x},\vec{y}\rangle,s} c^\dagger_{\circ,\vec{x},s} c_{\bullet,\vec{y},s} + c^\dagger_{\bullet,\vec{y},s} c_{\circ,\vec{x},s}. \tag{29}$$

To simplify the calculations, the sum over the nearest neighbours can be replaced with the sum over all lattice sites $\vec{x}$. In order to count each possible hopping of the electrons only once, the hopping is considered around the hexagon of one lattice site $\vec{x}$ in clockwise direction

$$\begin{aligned}\mathbb{H} = t \sum_{\vec{x},s} \Big(& c^\dagger_{\circ,\vec{x}+\frac{1}{3}\vec{a}_1+\frac{1}{3}\vec{a}_2,s} c_{\bullet,\vec{x}+\vec{v}_1,s} + c^\dagger_{\bullet,\vec{x}+\frac{1}{2}\vec{a}_1+\frac{1}{2}\vec{v}_2,s} c_{\circ,\vec{x}+\frac{1}{3}\vec{a}_1+\frac{1}{3}\vec{a}_2,s} + c^\dagger_{\circ,\vec{x}+\vec{v}_2,s} c_{\bullet,\vec{x}+\frac{1}{2}\vec{a}_1+\frac{1}{2}\vec{v}_2,s} \\ & + c^\dagger_{\bullet,\vec{x}-\frac{1}{3}\vec{a}_1-\frac{1}{3}\vec{a}_2,s} c_{\circ,\vec{x}+\vec{v}_2,s} + c^\dagger_{\circ,\vec{x}-\frac{1}{2}\vec{a}_1-\frac{1}{2}\vec{v}_2,s} c_{\bullet,\vec{x}-\frac{1}{3}\vec{a}_1-\frac{1}{3}\vec{a}_2,s} + c^\dagger_{\bullet,\vec{x}+\vec{v}_1,s} c_{\circ,\vec{x}-\frac{1}{2}\vec{a}_1-\frac{1}{2}\vec{v}_2,s} \Big). \end{aligned} \tag{30}$$

In order to diagonalize the Hamiltonian, we perform a Fourier transformation

$$\begin{aligned}\mathbb{H} \;=\; & t \sum_{\vec{x},s} \int_{-\frac{1}{2}}^{\frac{1}{2}} dk_1 \int_{-\frac{1}{2}}^{\frac{1}{2}} dk_2 \int_{-\frac{1}{2}}^{\frac{1}{2}} dk'_1 \int_{-\frac{1}{2}}^{\frac{1}{2}} dk'_2 \\ & \Bigg[c^\dagger_{\circ,s}(\vec{k}) \exp\left(-i\vec{k}\cdot\left(\vec{x}+\frac{1}{3}\vec{a}_1+\frac{1}{3}\vec{a}_2\right)\right) c_{\bullet,s}(\vec{k}') \exp\left(i\vec{k}'\cdot(\vec{x}+\vec{v}_1)\right) \\ & + c^\dagger_{\bullet,s}(\vec{k}) \exp\left(-i\vec{k}\cdot\left(\vec{x}+\frac{1}{2}\vec{a}_1+\frac{1}{2}\vec{v}_2\right)\right) c_{\circ,s}(\vec{k}') \exp\left(i\vec{k}'\cdot\left(\vec{x}+\frac{1}{3}\vec{a}_1+\frac{1}{3}\vec{a}_2\right)\right) \\ & + c^\dagger_{\circ,s}(\vec{k}) \exp\left(-i\vec{k}\cdot(\vec{x}+\vec{v}_2)\right) c_{\bullet,s}(\vec{k}') \exp\left(i\vec{k}'\cdot\left(\vec{x}+\frac{1}{2}\vec{a}_1+\frac{1}{2}\vec{v}_2\right)\right) \\ & + c^\dagger_{\bullet,s}(\vec{k}) \exp\left(-i\vec{k}\cdot\left(\vec{x}-\frac{1}{3}\vec{a}_1-\frac{1}{3}\vec{a}_2\right)\right) c_{\circ,s}(\vec{k}') \exp\left(i\vec{k}'\cdot(\vec{x}+\vec{v}_2)\right) \\ & + c^\dagger_{\circ,s}(\vec{k}) \exp\left(-i\vec{k}\cdot\left(\vec{x}-\frac{1}{2}\vec{a}_1-\frac{1}{2}\vec{v}_2\right)\right) c_{\bullet,s}(\vec{k}') \exp\left(i\vec{k}'\cdot\left(\vec{x}-\frac{1}{3}\vec{a}_1-\frac{1}{3}\vec{a}_2\right)\right) \\ & + c^\dagger_{\bullet,s}(\vec{k}) \exp\left(-i\vec{k}\cdot(\vec{x}+\vec{v}_1)\right) c_{\circ,s}(\vec{k}') \exp\left(i\vec{k}'\cdot\left(\vec{x}-\frac{1}{2}\vec{a}_1-\frac{1}{2}\vec{v}_2\right)\right) \Bigg]. \end{aligned} \tag{31}$$

Reordering the above equation, we can identify the δ-function of eq.(15)

$$
\begin{aligned}
\mathbb{H} &= t\frac{8\pi^2}{\sqrt{3}a^2}\sum_s \int_{-\frac{1}{2}}^{\frac{1}{2}} dk_1 \int_{-\frac{1}{2}}^{\frac{1}{2}} dk_2 \int_{-\frac{1}{2}}^{\frac{1}{2}} dk_1' \int_{-\frac{1}{2}}^{\frac{1}{2}} dk_2' \underbrace{\frac{\sqrt{3}a^2}{8\pi^2}\sum_{\vec{x}} \exp\left(i\vec{x}\cdot\left(\vec{k}'-\vec{k}\right)\right)}_{\delta(\vec{k}'-\vec{k})} \\
&\Bigg[c^\dagger_{\circ,s}(\vec{k}) c_{\bullet,s}(\vec{k}') \exp\left(-i\vec{k}\cdot\left(\frac{1}{3}\vec{a}_1+\frac{1}{3}\vec{a}_2\right)\right)\exp\left(i\vec{k}'\cdot\left(-\frac{1}{3}\vec{a}_1+\frac{2}{3}\vec{a}_2\right)\right) \\
&+c^\dagger_{\bullet,s}(\vec{k}) c_{\circ,s}(\vec{k}') \exp\left(-i\vec{k}\cdot\left(\frac{2}{3}\vec{a}_1-\frac{1}{3}\vec{a}_2\right)\right)\exp\left(i\vec{k}'\cdot\left(\frac{1}{3}\vec{a}_1+\frac{1}{3}\vec{a}_2\right)\right) \\
&+c^\dagger_{\circ,s}(\vec{k}) c_{\bullet,s}(\vec{k}') \exp\left(-i\vec{k}\cdot\left(\frac{1}{3}\vec{a}_1-\frac{2}{3}\vec{a}_2\right)\right)\exp\left(i\vec{k}'\cdot\left(\frac{2}{3}\vec{a}_1-\frac{1}{3}\vec{a}_2\right)\right) \\
&+c^\dagger_{\bullet,s}(\vec{k}) c_{\circ,s}(\vec{k}') \exp\left(-i\vec{k}\cdot\left(-\frac{1}{3}\vec{a}_1-\frac{1}{3}\vec{a}_2\right)\right)\exp\left(i\vec{k}'\cdot\left(\frac{1}{3}\vec{a}_1-\frac{2}{3}\vec{a}_2\right)\right) \\
&+c^\dagger_{\circ,s}(\vec{k}) c_{\bullet,s}(\vec{k}') \exp\left(-i\vec{k}\cdot\left(-\frac{2}{3}\vec{a}_1+\frac{1}{3}\vec{a}_2\right)\right)\exp\left(i\vec{k}'\cdot\left(-\frac{1}{3}\vec{a}_1-\frac{1}{3}\vec{a}_2\right)\right) \\
&+c^\dagger_{\bullet,s}(\vec{k}) c_{\circ,s}(\vec{k}') \exp\left(-i\vec{k}\cdot\left(-\frac{1}{3}\vec{a}_1+\frac{2}{3}\vec{a}_2\right)\right)\exp\left(i\vec{k}'\cdot\left(-\frac{2}{3}\vec{a}_1+\frac{1}{3}\vec{a}_2\right)\right)\Bigg]. \qquad (32)
\end{aligned}
$$

Performing the integral over the δ-function yields

$$
\begin{aligned}
\mathbb{H} &= t\frac{8\pi^2}{\sqrt{3}a^2}\sum_s \int_{-\frac{1}{2}}^{\frac{1}{2}} dk_1 \int_{-\frac{1}{2}}^{\frac{1}{2}} dk_2 \Bigg[c^\dagger_{\circ,s}(\vec{k}) c_{\bullet,s}(\vec{k}) \Bigg[\exp\left(2\pi i\left(\frac{2}{3}k_1-\frac{1}{3}k_2\right)\right) \\
&+\exp\left(2\pi i\left(-\frac{1}{3}k_1-\frac{1}{3}k_2\right)\right)+\exp\left(2\pi i\left(-\frac{1}{3}k_1+\frac{2}{3}k_2\right)\right)\Bigg] \\
&+c^\dagger_{\bullet,s}(\vec{k}) c_{\circ,s}(\vec{k}) \Bigg[\exp\left(-2\pi i\left(\frac{2}{3}k_1-\frac{1}{3}k_2\right)\right) \\
&+\exp\left(-2\pi i\left(-\frac{1}{3}k_1-\frac{1}{3}k_2\right)\right)+\exp\left(-2\pi i\left(-\frac{1}{3}k_1+\frac{2}{3}k_2\right)\right)\Bigg]\Bigg]. \qquad (33)
\end{aligned}
$$

Defining

$$
R(\vec{k}) = \exp\left(2\pi i\left(\frac{2}{3}k_1-\frac{1}{3}k_2\right)\right)+\exp\left(2\pi i\left(-\frac{1}{3}k_1-\frac{1}{3}k_2\right)\right)+\exp\left(2\pi i\left(-\frac{1}{3}k_1+\frac{2}{3}k_2\right)\right), \qquad (34)
$$

we obtain

$$
\begin{aligned}
\mathbb{H} &= t\frac{8\pi^2}{\sqrt{3}a^2}\sum_s \int_{-\frac{1}{2}}^{\frac{1}{2}} dk_1 \int_{-\frac{1}{2}}^{\frac{1}{2}} dk_2 \left(c^\dagger_{\circ,s}(\vec{k}) c_{\bullet,s}(\vec{k}) R(\vec{k}) + c^\dagger_{\bullet,s}(\vec{k}) c_{\circ,s}(\vec{k}) R^*(\vec{k})\right) \\
&= t\frac{\sqrt{3}a^2}{8\pi^2}\sum_s \int_B d^2k \left(c^\dagger_{\circ,s}(\vec{k}),\quad c^\dagger_{\bullet,s}(\vec{k})\right) \underbrace{\begin{bmatrix} 0 & R(\vec{k}) \\ R^*(\vec{k}) & 0 \end{bmatrix}}_{M} \begin{pmatrix} c_{\circ,s}(\vec{k}) \\ c_{\bullet,s}(\vec{k}) \end{pmatrix}. \qquad (35)
\end{aligned}
$$

The matrix $M \in (2\times 2, \mathbb{C})$ is Hermitian like the Hamiltonian itself. Thus it can be diagonalized with a unitary transformation. Since $R(\vec{k})$ is a complex number, it can be expressed as $R(\vec{k}) = \left|R(\vec{k})\right| e^{i\phi}$. The unitary matrix U then takes the form

$$
U = \frac{1}{\sqrt{2}}\begin{bmatrix} e^{-i\frac{\phi}{2}} & e^{i\frac{\phi}{2}} \\ e^{-i\frac{\phi}{2}} & -e^{i\frac{\phi}{2}} \end{bmatrix}. \qquad (36)
$$

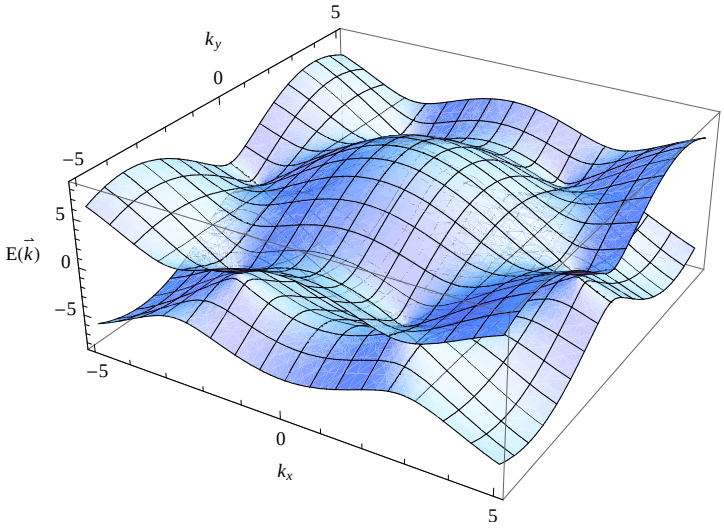

Figure 5: Energy spectrum of the electrons.

$$U \begin{bmatrix} 0 & R(\vec{k}) \\ R^*(\vec{k}) & 0 \end{bmatrix} U^\dagger = \begin{bmatrix} \left|R(\vec{k})\right| & 0 \\ 0 & -\left|R(\vec{k})\right| \end{bmatrix} \tag{37}$$

Hence the eigenvalues of the matrix M are $\pm\left|R(\vec{k})\right|$

$$\begin{aligned} \left|R(\vec{k})\right|^2 = R(\vec{k})R^*(\vec{k}) &= 3 + 2\cos(2\pi k_1) + 2\cos(2\pi k_2) + 2\cos(2\pi\,(k_1 - k_2)) \\ &= 3 + 4\cos(\frac{\sqrt{3}}{2}ak_y)\cos(\frac{a}{2}k_x) + 2\cos(ak_x). \end{aligned} \tag{38}$$

We made the transformation $k_1, k_2 \to k_x, k_y$ to get to eq.(38)

$$k_1 = \frac{a}{4\pi}k_x + \frac{\sqrt{3}a}{4\pi}k_y, \qquad k_2 = \frac{a}{2\pi}k_x. \tag{39}$$

Therefore the two energy bands of the Hamiltonian are $\pm t\left|R(\vec{k})\right|$ with

$$\left|R(\vec{k})\right| = \sqrt{3 + 4\cos(\frac{\sqrt{3}}{2}ak_y)\cos(\frac{a}{2}k_x) + 2\cos(ak_x)}. \tag{40}$$

They are plotted in figure 5 for $t = 2.8\,eV$ and $a = 1$.

3.3.1 Dirac Cones

Looking at the two energy bands from a different perspective, as it is done in figure 6, one sees a characteristic form. They are symmetric, and at the corners of the first Brillouin zone eq.(10), which are called Dirac points, their value is zero. Positive and negative energy values correspond to electrons and holes in the lattice. Hence there exists an electron-hole symmetry, or equivalently an $SU(2)_Q$ charge symmetry which was mentioned in section 3.2.4. The two bands are the valence and the conduction band. Since we are at half-filling, the valence band is completely filled, and the conduction band is empty when the electrons are in the ground state. The fact that those two bands touch each other at the Dirac points is responsible for graphene's semimetallic properties.

If we only consider low-energy values, cutting off the spectrum at high energies, as it is done in figure 7, the form of the energy band resembles cones, the so-called Dirac cones. To calculate the coordinates of these points, we have to set the energy to zero

$$\left|R(\vec{k})\right| = 0 \quad \Longleftrightarrow \quad \left|R(\vec{k})\right|^2 = 0, \tag{41}$$

$$\left|R(\vec{k})\right|^2 = 3 + 4\cos(\frac{\sqrt{3}}{2}ak_y)\cos(\frac{a}{2}k_x) + 2\cos(ak_x) = 0. \tag{42}$$

Choosing a certain corner of the Brillouin zone $k_x = \frac{2\pi}{3a}$ and $k_y = \frac{2\pi}{\sqrt{3}a}$ is a result of the above equation. Only two corners hold independent information, the coordinates of these points are for example

$$\vec{K}_\pm = \pm\frac{2\pi}{\sqrt{3}a}\begin{pmatrix}\frac{1}{\sqrt{3}}\\ 1\end{pmatrix}. \tag{43}$$

When we expand the energy values around the points $\vec{K}_\pm$ we get the Dirac cones

$$\begin{aligned}
R^2(\vec{K}_+ + \delta\vec{k}) &= R^2(\vec{K}_+) + \left.\frac{\partial R^2(\vec{k})}{\partial k_x}\right|_{\vec{K}_+}\delta k_x + \left.\frac{\partial R^2(\vec{k})}{\partial k_y}\right|_{\vec{K}_+}\delta k_y \\
&+ \frac{1}{2}\left.\frac{\partial^2 R^2(\vec{k})}{\partial {k_x}^2}\right|_{\vec{K}_+}\delta k_x^2 + \frac{1}{2}\left.\frac{\partial^2 R^2(\vec{k})}{\partial {k_y}^2}\right|_{\vec{K}_+}\delta k_y^2 + \left.\frac{\partial^2 R^2(\vec{k})}{\partial k_x \partial k_y}\right|_{\vec{K}_+}\delta k_x\delta k_y + \mathcal{O}({\delta\vec{k}}^3) \\
&\approx 0 + \left(-4\cos\left(\frac{\sqrt{3}}{2}ak_y\right)\frac{a}{2}\sin\left(\frac{a}{2}k_x\right)\Big|_{\vec{K}_+} - 2a\sin(ak_x)|_{\vec{K}_+}\right)\delta k_x \\
&+ \left(-4\cos\left(\frac{a}{2}k_x\right)\frac{\sqrt{3}}{2}a\sin\left(\frac{\sqrt{3}}{2}ak_y\right)\Big|_{\vec{K}_+}\right)\delta k_y \\
&+ \left(-\frac{1}{2}4\cos\left(\frac{\sqrt{3}}{2}ak_y\right)\left(\frac{a}{2}\right)^2\cos\left(\frac{a}{2}k_x\right)\Big|_{\vec{K}_+} - 2a^2\cos(ak_x)|_{\vec{K}_+}\right)\delta k_x^2 \\
&+ \left(-\frac{1}{2}4\cos\left(\frac{a}{2}k_x\right)\left(\frac{\sqrt{3}}{2}a\right)^2\cos\left(\frac{\sqrt{3}}{2}ak_y\right)\Big|_{\vec{K}_+}\right)\delta k_y^2 \\
&+ \left(4\sin\left(\frac{a}{2}k_x\right)\frac{a}{2}\frac{\sqrt{3}}{2}a\sin\left(\frac{\sqrt{3}}{2}ak_y\right)\Big|_{\vec{K}_+}\right)\delta k_x\delta k_y \\
&= \frac{3}{4}a^2\left|\delta\vec{k}\right|^2.
\end{aligned} \tag{44}$$

Hence the energy is

$$E(\vec{K}_+ + \delta\vec{k}) = \pm t\frac{a}{2}\sqrt{3}\left|\delta\vec{k}\right| = \pm\underbrace{\frac{a\sqrt{3}t}{2\hbar}}_{v_F}\left|\delta\vec{p}\right| \tag{45}$$

$$\Longrightarrow E(\vec{p}) = \pm v_F\left|\delta\vec{p}\right|. \tag{46}$$

We identified the Fermi velocity $v_F = \frac{a\sqrt{3}t}{2\hbar} \approx 9\cdot 10^5\,\frac{m}{s}$ in eq.(45). This is a very high velocity; about 300 times less than the speed of light, and it does not depend on the momentum of the electrons. The dispersion relation is very interesting since electrons usually have a quadratic dispersion relation. On the other hand, a linear dispersion relation is characteristic for massless particles, such as photons. Spin $\frac{1}{2}$-particles with such an energy dispersion relation are called Dirac fermions. So these low-energy electrons have peculiar properties, generated by the geometry of the honeycomb lattice. We must treat them as relativistic massless particles.

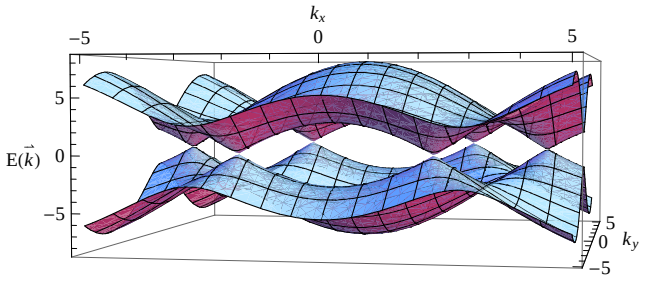

Figure 6: Illustration of the energy spectrum.

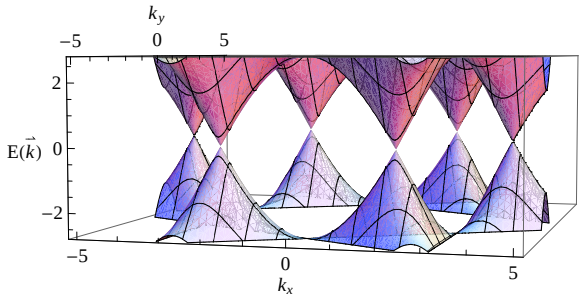

Figure 7: Illustration of the Dirac cones.

3.4 Hopping to Next-to-Nearest Neighbours

Electrons may also hop to next-to-nearest neighbours. If we want to account for this, we must add an additional term to the Hubbard Hamiltonian with a different hopping parameter t'. To diagonalize the additional term, we perform an analogous Fourier transformation. It is already diagonal after the transformation, since the electrons stay on the same sublattice while hopping to next-to-nearest neighbours. The full Hamiltonian now looks as follows

$$\mathbb{H} = t \sum_{\langle \vec{x},\vec{y}\rangle,s} \left(c^\dagger_{\circ,\vec{x},s} c_{\bullet,\vec{y},s} + c^\dagger_{\bullet,\vec{y},s} c_{\circ,\vec{x},s} \right) + t' \sum_{\langle \vec{x},\vec{z}\rangle,s} \left(c^\dagger_{\circ,\vec{x},s} c_{\circ,\vec{z},s} + c^\dagger_{\bullet,\vec{x},s} c_{\bullet,\vec{z},s} \right). \tag{47}$$

Here, $\langle \vec{x},\vec{z}\rangle$ is a pair of next-to-nearest neighbours on one of the two sublattices. We will now diagonalize the new Hamiltonian. It is sufficient to make the calculation for one of the two added terms. Therefore the indices $\circ$ or $\bullet$ will be neglected in the next steps. As already mentioned, the method is the same as for the Hamiltonian which considers only nearest neighbour hopping

$$\begin{aligned}
\mathbb{H} &= t' \sum_{\vec{x},s} c^\dagger_{\vec{x}+\vec{v}_1,s} c_{\vec{x}+\vec{v}_1+\vec{a}_1-\vec{a}_2,s} + c^\dagger_{\vec{x}+\vec{v}_1+\vec{a}_1-\vec{a}_2,s} c_{\vec{x}+\vec{v}_1,s} \\
&\quad + c^\dagger_{\vec{x}+\vec{v}_1,s} c_{\vec{x}+\vec{v}_1-\vec{a}_2,s} + c^\dagger_{\vec{x}+\vec{v}_1-\vec{a}_2,s} c_{\vec{x}+\vec{v}_1,s} \\
&\quad + c^\dagger_{\vec{x}+\vec{v}_1+\vec{a}_1-\vec{a}_2,s} c_{\vec{x}+\vec{v}_1-\vec{a}_2,s} + c^\dagger_{\vec{x}+\vec{v}_1-\vec{a}_2,s} c_{\vec{x}+\vec{v}_1+\vec{a}_1-\vec{a}_2,s} \\
&= t' \frac{\sqrt{3}a^2}{8\pi^2} \int_B d^2k \quad c^\dagger_s(\vec{k}) c_s(\vec{k}) \underbrace{4\cos\left(\frac{\sqrt{3}}{2}ak_y\right)\cos\left(\frac{a}{2}k_x\right) + 2\cos\left(ak_x\right)}_{\left|R(\vec{k})\right|^2 - 3}.
\end{aligned} \tag{48}$$

Taking the Hamiltonian of eq.(35) and inserting the additional part we get

$$\mathbb{H} = \frac{\sqrt{3}a^2}{8\pi^2} \sum_s \int_B d^2k \begin{pmatrix} c^\dagger_{\circ,s}(\vec{k}), & c^\dagger_{\bullet,s}(\vec{k}) \end{pmatrix} \begin{bmatrix} t'\left(\left|R(\vec{k})\right|^2 - 3\right) & tR(\vec{k}) \\ tR^*(\vec{k}) & t'\left(\left|R(\vec{k})\right|^2 - 3\right) \end{bmatrix} \begin{pmatrix} c_{\circ,s}(\vec{k}) \\ c_{\bullet,s}(\vec{k}) \end{pmatrix}. \tag{49}$$

The diagonalization of this Hamilton yields the energy eigenvalues

$$E_\pm(\vec{k}) = t'\left(\left|R(\vec{k})\right|^2 - 3\right) \pm t\left|R(\vec{k})\right|. \tag{50}$$

The eigenvalues are plotted in figure 8 with $t = 2.8\,eV$, $t' = 1eV$ and $a = 1$. As one can see, the symmetry between positive and negative energy values is broken. However for low energies, the symmetry holds, and the energy bands still have the form of Dirac cones.

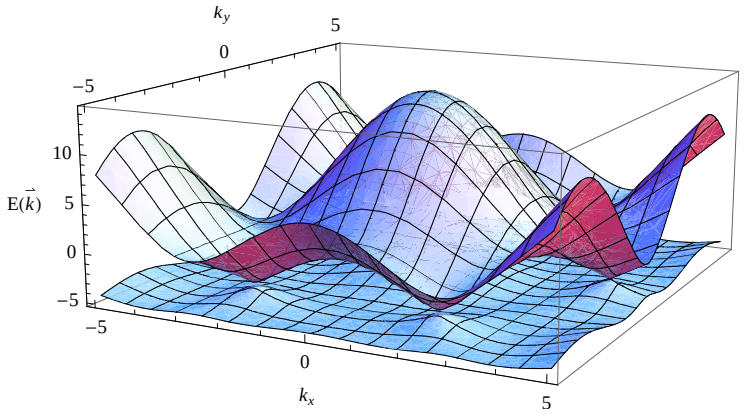

Figure 8: Energy spectrum of the electrons if hopping to next-to-nearest neighbours is allowed.

4 Effective Low-Energy Field Theory

Effective theories are very useful to understand the physics of a certain range of energy in which they appropriately describe the relevant physical processes. A fundamental theory, a microscopic model, is the basis to construct the effective theory. Since in the effective theory only the degrees of freedom relevant in a certain domain of energy are included, this theory is simpler. Therefore the physics it describes, can be calculated more easily i.e. effectively compared to the fundamental theory, which, on the other hand, is valid for all energies, but which is often only numerically solvable. The effective theory is equivalent to the microscopic model in the chosen range of energy.

In this section, an effective theory for low energies is derived based on the Hubbard model. Although the effective theory could be constructed generally by the determination of the degrees of freedom, and the symmetries of the Hubbard model, in this case, it is straightforward to derive the effective Hamiltonian from an expansion of the Hubbard Hamiltonian eq.(35) around the Dirac points, where the energy is equal to zero. Before the calculations are presented, the Dirac equation is introduced, so that one can put the effective Hamiltonian into the appropriate context.

4.1 Dirac Equation

In quantum mechanics particles are described by wave functions ψ. The Schrödinger equation is used to compute the energy of particles, but the Schrödinger equation is not valid in the relativistic regime. Paul Dirac found the "relativistic Schrödinger equation" for spin $\frac{1}{2}$-particles in 1928, the Dirac equation:

$$i\hbar\frac{\partial\psi}{\partial t} = \left(\beta mc^2 + \vec{\alpha}\cdot\vec{p}c\right)\psi. \tag{51}$$

$$\alpha_i = \begin{bmatrix} 0 & \sigma_i \\ \sigma_i & 0 \end{bmatrix}, \qquad \beta = \begin{pmatrix} \mathbb{1}_2 & 0 \\ 0 & -\mathbb{1}_2 \end{pmatrix} \tag{52}$$

$$\sigma_1 = \begin{pmatrix} 0 & 1 \\ 1 & 0 \end{pmatrix}, \qquad \sigma_2 = \begin{pmatrix} 0 & -i \\ i & 0 \end{pmatrix}, \qquad \sigma_3 = \begin{pmatrix} 1 & 0 \\ 0 & -1 \end{pmatrix} \tag{53}$$

Here, σ_i are the Pauli matrices and ψ is a Dirac spinor with four components. This equation is valid in four-dimensional space-time. Unlike the Schrödinger equation, the Dirac equation only has derivatives of first order, in both space and time.

4.2 Effective Hamiltonian

When we diagonalized the Hamiltonian of eq.(35), we got a (2×2) matrix M. All the information about the energy is stored in it. Thus, if we expand it about $\vec{K}_+$, we can derive the effective Hamiltonian for graphene for low energies. The matrix M has the following form

$$M = \begin{pmatrix} 0 & R(\vec{k}) \\ R^*(\vec{k}) & 0 \end{pmatrix}. \tag{54}$$

Remembering also $R(\vec{k})$, and the coordinates of $\vec{K}_+$

$$R(\vec{k}) = \exp\left(\frac{ia}{\sqrt{3}}k_y\right) + \exp\left(-\frac{ia}{2\sqrt{3}}k_y - \frac{ia}{2}k_x\right) + \exp\left(-\frac{ia}{2\sqrt{3}}k_y + \frac{ia}{2}k_x\right) \tag{55}$$

$$\vec{K}_+ = \frac{2\pi}{\sqrt{3}a}\begin{bmatrix} \frac{1}{\sqrt{3}} \\ 1 \end{bmatrix}, \tag{56}$$

we can expand $R(\vec{k})$ about $\vec{K}_+$ up to first order which yields

$$\begin{aligned} R(\vec{K}_+ + \delta\vec{k}) &= \exp\left(\frac{2\pi i}{3}\right)\exp\left(\frac{ia}{\sqrt{3}}\delta k_y\right) + \exp\left(-\frac{2\pi i}{3}\right)\exp\left(-\frac{ia}{2\sqrt{3}}\delta k_y - \frac{ia}{2}\delta k_x\right) \\ &\quad + \exp\left(-\frac{ia}{2\sqrt{3}}\delta k_y + \frac{ia}{2}\delta k_x\right) \\ &\approx \frac{a}{2}\sqrt{3}\left(-\frac{i}{2}\delta k_y + \frac{\sqrt{3}i}{2}\delta k_x - \frac{\sqrt{3}}{2}\delta k_y - \frac{1}{2}\delta k_x\right) \\ &= \frac{\sqrt{3}a}{2\hbar}\left(-\frac{i}{2}\delta q_y + \frac{\sqrt{3}i}{2}\delta q_x - \frac{\sqrt{3}}{2}\delta q_y - \frac{1}{2}\delta q_x\right). \end{aligned} \tag{57}$$

Above we set $\hbar\vec{k} = \vec{q}$. Rotating the coordinate system by 240°

$$\begin{pmatrix} p_x \\ p_y \end{pmatrix} = \begin{bmatrix} \cos\left(\frac{4\pi}{3}\right) & \sin\left(\frac{4\pi}{3}\right) \\ -\sin\left(\frac{4\pi}{3}\right) & \cos\left(\frac{4\pi}{3}\right) \end{bmatrix} \begin{pmatrix} q_x \\ q_y \end{pmatrix}, \tag{58}$$

we obtain

$$R(\vec{p}) \approx \frac{\sqrt{3}a}{2\hbar}\left(p_x + ip_y\right), \tag{59}$$

and complex conjugation yields

$$R^*(\vec{p}) \approx \frac{\sqrt{3}a}{2\hbar}\left(p_x - ip_y\right). \tag{60}$$

We can write the Hamiltonian of eq.(35) as

$$\begin{aligned} \mathbb{H} &\approx t\frac{\sqrt{3}a^2}{8\pi^2\hbar^2}\sum_s\int_B d^2p\begin{pmatrix} c^\dagger_{\circ,s}(\vec{p}), & c^\dagger_{\bullet,s}(\vec{p}) \end{pmatrix}\frac{\sqrt{3}a}{2\hbar}\begin{bmatrix} 0 & p_x + ip_y \\ p_x - ip_y & 0 \end{bmatrix}\begin{pmatrix} c_{\circ,s}(\vec{p}) \\ c_{\bullet,s}(\vec{p}) \end{pmatrix} \\ &= \frac{\sqrt{3}a^2}{8\pi^2\hbar^2}\sum_s\int_B d^2p\begin{pmatrix} c^\dagger_{\circ,s}(\vec{p}), & c^\dagger_{\bullet,s}(\vec{p}) \end{pmatrix}\frac{\sqrt{3}at}{2\hbar}\underbrace{\begin{pmatrix}\sigma_1, & -\sigma_2\end{pmatrix}}_{\vec{\alpha}'}\begin{pmatrix} p_x \\ p_y \end{pmatrix}\begin{pmatrix} c_{\circ,s}(\vec{p}) \\ c_{\bullet,s}(\vec{p}) \end{pmatrix} \\ &= \frac{\sqrt{3}a^2}{8\pi^2\hbar^2}\sum_s\int_B d^2p\begin{pmatrix} c^\dagger_{\circ,s}(\vec{p}), & c^\dagger_{\bullet,s}(\vec{p}) \end{pmatrix}\underbrace{v_F\,\vec{\alpha}'\cdot\vec{p}}_{H_{D'}}\begin{pmatrix} c_{\circ,s}(\vec{p}) \\ c_{\bullet,s}(\vec{p}) \end{pmatrix}. \end{aligned} \tag{61}$$

We derived the Dirac equation for the point $\vec{K}_+$. In order to account for the whole energy of the system, we must also compute the energy at the point $\vec{K}_-$. The calculation is analogous to the one at $\vec{K}_+$, except that we must rotate the coordinate system by 60°

$$\begin{aligned} & R(\vec{K}_- + \delta\vec{k}) = \frac{\sqrt{3}a}{2\hbar}(p_x - ip_y), \qquad R^*(\vec{K}_- + \delta\vec{k}) = \frac{\sqrt{3}a}{2\hbar}(p_x + ip_y), \\ \mathbb{H} &= \frac{\sqrt{3}a^2}{8\pi^2\hbar^2}\sum_s\int_B d^2p\begin{pmatrix} c^\dagger_{\circ,s}(\vec{p}), & c^\dagger_{\bullet,s}(\vec{p}) \end{pmatrix}\frac{\sqrt{3}at}{2\hbar}\underbrace{\begin{pmatrix}\sigma_1, & \sigma_2\end{pmatrix}}_{\vec{\alpha}}\begin{pmatrix} p_x \\ p_y \end{pmatrix}\begin{pmatrix} c_{\circ,s}(\vec{p}) \\ c_{\bullet,s}(\vec{p}) \end{pmatrix} \\ &= \frac{\sqrt{3}a^2}{8\pi^2\hbar^2}\sum_s\int_B d^2p\begin{pmatrix} c^\dagger_{\circ,s}(\vec{p}), & c^\dagger_{\bullet,s}(\vec{p}) \end{pmatrix}\underbrace{v_F\,\vec{\alpha}\cdot\vec{p}}_{H_D}\begin{pmatrix} c_{\circ,s}(\vec{p}) \\ c_{\bullet,s}(\vec{p}) \end{pmatrix}. \end{aligned} \tag{62}$$

If we compare the two Dirac Hamiltonians $H_{D'}$ and H_D with the Dirac eq.(51), we can see that they have a similar term $v_F\,\vec{\alpha}\cdot\vec{p}$, but no diagonal term βmc^2, which makes sense since the electrons behave like particles without mass. Here α_i is a (2×2) matrix only, compared to the (4×4) matrix α_i in the Dirac equation. This results from the fact that graphene is a two-dimensional material, and thus the above equations were calculated in three-dimensional space-time. The two components of the effective Dirac spinors account for the two sublattices $\circ, \bullet$. So we actually derived an effective theory of two two-dimensional Dirac spinors.

5 Introduction of a Magnetic Field

The properties of graphene in a magnetic field are very interesting. They have been researched intensely, particularly since the half-integer quantum Hall effect was discovered. In this section, a constant magnetic field is introduced which acts on the electrons. The energy spectrum of the electrons is again calculated with the Hubbard model, but also with the effective theory. The magnetic field causes the energy to quantize into discrete energy levels; the Landau levels. A magnetic field, perpendicular to the graphene layer, pointing in the $z-$direction, is introduced and a vector potential is chosen accordingly:

$$\vec{B} = \begin{pmatrix} 0 \\ 0 \\ B \end{pmatrix}, \qquad \vec{A} = \begin{pmatrix} -Bx_2 \\ 0 \\ 0 \end{pmatrix}. \tag{63}$$

5.1 Pauli Equation

The Pauli equation describes the time evolution of non-relativistic spin $\frac{1}{2}$-particles. It differs form the Schrödinger equation because it includes an additional term, which takes into account the interactions between the spin of the particle and an external magnetic field. It is derived in the calculations below by taking the non-relativistic limit ($|\vec{p}| \ll mc^2$) of the Dirac eq.(51)

$$i\hbar\partial_t\psi = (\vec{\alpha}\cdot\vec{p}c + \beta mc^2)\psi = \left(\frac{\hbar c}{i}\vec{\alpha}\cdot\vec{\nabla} + \beta mc^2\right)\psi.$$

with $\vec{\alpha}$ and β defined as in eqs. (52) and (53) and $\vec{p} = -i\hbar\vec{\nabla}$. In the next step the covariant derivatives which account for a minimal coupling to an electromagnetic field

$$D_t = \partial_t + \frac{ie}{\hbar}\phi, \qquad \vec{D} = \vec{\nabla} - \frac{ie}{\hbar c}\vec{A}, \tag{64}$$

must be introduced, such that the Dirac equation stays invariant under gauge transformations. The Dirac equation now reads

$$i\hbar D_t\psi = \frac{\hbar c}{i}\vec{\alpha}\cdot\vec{D}\psi + \beta mc^2\psi. \tag{65}$$

The Dirac spinor ψ, which has four components, can be expressed as

$$\psi = \begin{pmatrix} u \\ v \end{pmatrix} \tag{66}$$

with u denoting the two components of the particle and v of the antiparticle. Thus the Dirac equation takes the following form

$$i\hbar\partial_t \begin{pmatrix} u \\ v \end{pmatrix} = e\phi \begin{pmatrix} u \\ v \end{pmatrix} + \left(\frac{\hbar c}{i}\vec{\sigma}\cdot\vec{\nabla} - e\vec{\sigma}\cdot\vec{A}\right)\begin{pmatrix} v \\ u \end{pmatrix} + mc^2 \begin{pmatrix} u \\ -v \end{pmatrix}. \tag{67}$$

If we write

$$\begin{pmatrix} u \\ v \end{pmatrix} = \exp\left(\frac{-imc^2}{\hbar}t\right)\begin{pmatrix} \varphi \\ \chi \end{pmatrix}, \tag{68}$$

and insert the second component of eq.(68) into the second component of the Dirac equation we obtain

$$i\hbar\left(\frac{-imc^2}{\hbar}\right)\chi + i\hbar\partial_t\chi = e\phi\chi + \frac{\hbar c}{i}\vec{\sigma}\cdot\vec{\nabla}\varphi - e\vec{\sigma}\cdot\vec{A}\varphi - mc^2\chi. \tag{69}$$

Taking the non-relativistic limit, which means assuming, that the time-dependence is mostly in the phase factor, we can express χ in the following way

$$\chi = \frac{\frac{\hbar c}{i}\vec{\sigma}\cdot\vec{\nabla} - e\vec{\sigma}\cdot\vec{A}}{2mc^2}\varphi = \frac{\hbar\vec{\sigma}\cdot\vec{D}}{2imc}\varphi. \tag{70}$$

Inserting this expression into the first component of the Dirac equation yields

$$i\hbar\partial_t\varphi = e\phi\varphi + \frac{1}{2mc^2}\left(\frac{\hbar c}{i}\vec{\sigma}\cdot\vec{\nabla} - e\vec{\sigma}\cdot\vec{A}\right)^2\varphi = e\phi\varphi - \frac{\hbar^2}{2m}\left(\vec{\sigma}\cdot\vec{D}\right)^2\varphi. \tag{71}$$

To compute $\left(\vec{\sigma}\cdot\vec{D}\right)^2\varphi$ we use

$$\sigma_i\sigma_j = \delta_{ij} + i\epsilon_{ijk}\sigma_k, \tag{72}$$

whicht leads to

$$\left(\vec{\sigma}\cdot\vec{D}\right)^2\varphi = \left(\vec{D}^2 + \frac{e}{\hbar c}\vec{\sigma}\cdot\vec{B}\right)\varphi. \tag{73}$$

Finally, we derived the Pauli equation

$$i\hbar\partial_t\varphi = \left(\underbrace{e\phi + \frac{1}{2m}\left(\vec{p} - \frac{e}{c}\vec{A}\right)^2}_{\text{Schrödinger term}} \quad \underbrace{-\frac{e\hbar}{2mc}\vec{\sigma}\cdot\vec{B}}_{\text{Stern-Gerlach term}}\right)\varphi, \tag{74}$$

where we can immediately see the additional Stern-Gerlach term. It was pointed out by Fröhlich and Studer [7] that the Pauli equation, when two higher order terms are added, can be written in a form which is invariant under local $SU(2)_S \otimes U(1)_Q$ gauge transformations. Thus the Pauli equation can be written as follows

$$i\hbar D_t\,\psi = \mathbb{H}_P\,\psi, \tag{75}$$

where

$$D_t = \partial_t - \frac{ie}{\hbar}\phi - \frac{ie}{2m_e c}\vec{\sigma}\cdot\vec{B} + \frac{ie\hbar}{8m^2c^2}\vec{\nabla}\cdot\vec{E}, \qquad \mathbb{H}_P = -\frac{1}{2m}\left(\vec{\nabla} + \frac{ie}{c}\vec{A}\right)^2 - \frac{ie\hbar^2}{8m_e^2c^2}\vec{E}\times\vec{\sigma}. \tag{76}$$

The contribution of Fröhlich and Studer is very significant in many aspects, particularly, it determines how the Hamiltonian of the Hubbard model must be altered in order to take into consideration the coupling of the electrons to the external magnetic field.

5.2 Applying a Magnetic Field to the Hubbard Model

We compute the energies of the electrons by accounting for nearest neighbour hopping as in the Hamiltonian eq.(19), but the Hamiltonian must now be modified by an $SU(2)_S \otimes U(1)_Q$ parallel transporter $U_{\vec{y},\vec{z}}$. This phase $U_{\vec{y},\vec{z}}$ is defined as

$$U_{\vec{y},\vec{z}} = \exp\left(\frac{ie}{\hbar}\int_{\vec{y}}^{\vec{z}} d\vec{x}\,\vec{A}(\vec{x})\right) \quad \in U(1). \tag{77}$$

The parallel transporter $U_{\vec{y},\vec{z}}$ and the creation respectively annihilation operators are changed by the gauge transformation $\vec{A}(\vec{x}) \to \vec{A}(\vec{x})' = \vec{A}(\vec{x}) + \vec{\nabla}\varphi(\vec{x})$ in the following way

$$U_{\vec{y},\vec{z}} \to U'_{\vec{y},\vec{z}} = U_{\vec{y},\vec{z}}\,\exp\left(\frac{ie}{\hbar}\varphi(\vec{y})\right)\exp\left(-\frac{ie}{\hbar}\varphi(\vec{z})\right), \tag{78}$$

$$c_{\vec{y}} \to c'_{\vec{y}} = c_{\vec{y}}\,\exp\left(\frac{ie}{\hbar}\varphi(\vec{y})\right), \qquad c^\dagger_{\vec{y}} \to c^{\dagger\prime}_{\vec{y}} = c^\dagger_{\vec{y}}\,\exp\left(-\frac{ie}{\hbar}\varphi(\vec{y})\right). \tag{79}$$

Because of the parallel transporter, the Hamiltonian of eq.(19) is invariant under the gauge transformation, which can now easily be shown. Since there is a line integral in the exponential of the parallel transporter, the transporter depends on the vector potential and differs for non-identical lattice sites $\vec{y},\vec{z}$. A hexagon at the position $\vec{x}$ has in total six parallel transporters (see figure 9) although by calculating them, one finds that there are only three being non-identical

$$U_1 = 1, \quad U_2 = \exp\left(i\vec{q}\cdot\vec{x} - i\varphi\right), \quad U_3 = \exp\left(-i\vec{q}\cdot\vec{x} - i\varphi\right), \tag{80}$$

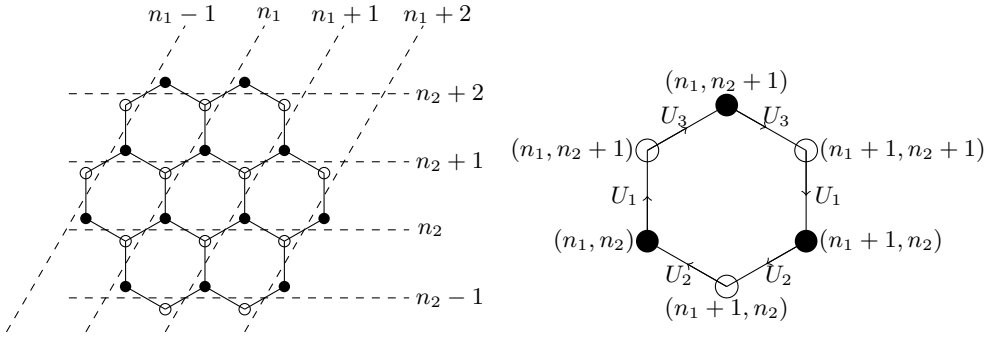

Figure 9: New labeling of the honeycomb lattice with its parallel transporters.

where $\vec{q}$ and φ are defined by

$$\vec{q} = \begin{pmatrix} 0 \\ 1 \end{pmatrix} \frac{aBe}{2\hbar}, \qquad \varphi = \frac{\sqrt{3}ea^2B}{8\hbar}. \tag{81}$$

Taking a close look, one notices that the parallel transporters do not depend on x_1, and hence they are invariant under a translation in this direction. This is not the case for the x_2 direction. A new labeling of the lattice sites is introduced in figure 9; instead of a vector $\vec{x} = n_1\vec{a}_1 + n_2\vec{a}_2$, which points to the middle of a hexagon and a translation vector $\vec{v}_i$, which points to the actual lattice site, each site is labeled with two integers (n_1, n_2). The Hamiltonian can be written as

$$\begin{aligned} \mathbb{H} = t \sum_{n_1,n_2,s} \quad & c^\dagger_{(n_1+1,n_2)\circ,s}\, U_1\, c_{(n_1+1,n_2+1)\bullet,s} + c^\dagger_{(n_1+1,n_2)\bullet,s}\, U_2\, c_{(n_1+1,n_2)\circ,s} + \\ & c^\dagger_{(n_1,n_2)\circ,s}\, U_2\, c_{(n_1+1,n_2)\bullet,s} + c^\dagger_{(n_1,n_2+1)\bullet,s}\, U_1\, c_{(n_1,n_2+1)\circ,s} + \\ & c^\dagger_{(n_1,n_2+1)\circ,s}\, U_3\, c_{(n_1,n_2+1)\bullet,s} + c^\dagger_{(n_1+1,n_2+1)\bullet,s}\, U_3\, c_{(n_1,n_2+1)\circ,s}. \end{aligned} \tag{82}$$

To diagonalize the Hamiltonian without a magnetic field, we performed a two-dimensional Fourier transformation. Taking into consideration the magnetic field, we will only perform the Fourier transformation in the x_1 direction since the Hamiltonian is invariant under translation operations in this direction only. Below the Fourier transformation of the annihilation and creation operators is shown

$$c_{(n_2)s}(k_x) = \sum_{n_1} c_{(n_1,n_2),s} \exp\left(ik_x a n_1\right), \qquad c^\dagger_{(n_2)s}(k_x) = \sum_{n_1} c^\dagger_{(n_1,n_2),s} \exp\left(-ik_x a n_1\right), \tag{83}$$

as well as the inverse Fourier transformation

$$c_{(n_1,n_2),s} = \frac{a}{2\pi} \int_{-\frac{\pi}{a}}^{\frac{\pi}{a}} dk_x c_{(n_2),s}(k_x) \exp\left(-ik_x a n_1\right), \qquad c^\dagger_{(n_1,n_2),s} = \frac{a}{2\pi} \int_{-\frac{\pi}{a}}^{\frac{\pi}{a}} dk_x c^\dagger_{(n_2),s}(k_x) \exp\left(ik_x a n_1\right). \tag{84}$$

The next calculation is similar to the ones without any magnetic field. We must also identify a δ-function to simplify the Hamiltonian, which then has the following form

$$\begin{aligned}\mathbb{H} = \sum_{n_2,s}\left(\frac{a}{2\pi}\right)\int_{-\frac{\pi}{a}}^{\frac{\pi}{a}} dk_x \quad \Bigg[\quad & c^\dagger_{(n_2)\circ,s}(k_x)c_{(n_2+1)\bullet,s}(k_x) + \\ & c^\dagger_{(n_2)\bullet,s}(k_x)c_{(n_2)\circ,s}(k_x)\exp\left(i\varphi(2n_2-1)\right) + \\ & c^\dagger_{(n_2)\circ,s}(k_x)c_{(n_2)\bullet,s}(k_x)\exp\left(i\varphi(2n_2-1)-ik_xa\right) + \\ & c^\dagger_{(n_2+1)\bullet,s}(k_x)c_{(n_2)\circ,s}(k_x) + \\ & c^\dagger_{(n_2+1)\circ,s}(k_x)c_{(n_2+1)\bullet,s}(k_x)\exp\left(-i\varphi(2n_2-1)\right) + \\ & c^\dagger_{(n_2+1)\bullet,s}(k_x)c_{(n_2+1)\circ,s}(k_x)\exp\left(-i\varphi(2n_2-1)+ik_xa\right)\Bigg]. \end{aligned} \tag{85}$$

To solve the eigenvalue problem $E\,|\psi\rangle = \mathbb{H}\,|\psi\rangle$, one acts with the above Hamiltonian on the following eigenvector

$$|\psi\rangle = \sum_{n_2} a_{(n_2)\circ,s}(k_x)\, c^\dagger_{(n_2)\circ,s}(k_x) + a_{(n_2)\bullet,s}(k_x)\, c^\dagger_{(n_2)\bullet,s}(k_x). \tag{86}$$

Comparing the coefficients of the creation operators, and defining two new functions $g(k_x) = \exp\left(ik_x\frac{a}{2}\right)$ and $h(k_x,n_2) = 2\cos\left(2\varphi n_2 - \varphi - k_x\frac{a}{2}\right)$, one obtains the two recursive relations

$$\frac{E}{t}a_{(n_2)\circ,s}(k_x) = a_{(n_2+1)\bullet,s}(k_x) + a_{(n_2)\bullet,s}g(k_x)^*h(k_x,n_2), \tag{87}$$

$$\frac{E}{t}a_{(n_2)\bullet,s}(k_x) = a_{(n_2-1)\circ,s}(k_x) + a_{(n_2)\circ,s}g(k_x)h(k_x,n_2). \tag{88}$$

Those two relations can also be written as a matrix equation

$$\begin{bmatrix} \cdot & & & & & & & \cdot \\ & \cdot & & & & & \cdot & \\ & & \cdot & & & \cdot & & \\ & & & 0 & 1 & & & \\ & & & 1 & 0 & gh & & \\ & & & & g^*h & 0 & 1 & \\ & & & & & 1 & 0 & \\ & & \cdot & & & & & \cdot \\ & \cdot & & & & & \cdot & \\ \cdot & & & & & & & \cdot \end{bmatrix} \begin{pmatrix} \cdot \\ \cdot \\ \cdot \\ a_{(n_2-1)\circ,s} \\ a_{(n_2)\bullet,s} \\ a_{(n_2)\circ,s} \\ a_{(n_2+1)\bullet,s} \\ \cdot \\ \cdot \\ \cdot \end{pmatrix} = \frac{E}{t} \begin{pmatrix} \cdot \\ \cdot \\ \cdot \\ a_{(n_2-1)\circ,s} \\ a_{(n_2)\bullet,s} \\ a_{(n_2)\circ,s} \\ a_{(n_2+1)\bullet,s} \\ \cdot \\ \cdot \\ \cdot \end{pmatrix}, \tag{89}$$

where the dependence of the functions g and h on k_x and n_2 has been suppressed. This problem can only be solved numerically. This has been done in the paper [2]. For the energy value $E = 0$, the eigenvalue problem decouples on each sublattice, which simplifies the problem. By making it finite, for example setting $a_{(-1)}(k_x) = 0$ and $a_{(0)}(k_x) = 1$, one can write down the eigenvectors as a product of the two functions $g(k_x)$ and $h(k_x,n)$. This has not been pursued further in this thesis because it led to results which could not be compared with those of the effective theory.

5.3 Energy Levels of the Electrons in an External Magnetic Field Calculated with the Effective Theory

To compute the energy spectrum, we take the Hamiltonians of the effective theory $H_{D'}$ (61) and H_D (62), derived earlier. The energies must be computed separately for each Dirac cone because

the effective Hamiltonian has a slightly different form for each one. We start with the Hamiltonian H_D around the Dirac point $\vec{K}_-$

$$\mathbb{H} = v_F \vec{\alpha} \cdot \vec{p}, \qquad \vec{\alpha} = (\sigma_1, \sigma_2). \tag{90}$$

Here σ_i are the Pauli matrices of eq.(53). We will now insert the quantum mechanical momentum $\vec{p} = -i\hbar\vec{D}$ with the covariant derivatives eq.(64) to account for the magnetic field

$$\mathbb{H} = v_F \begin{bmatrix} 0 & -i\hbar\partial_x + \frac{ie}{c}Bx - \hbar\partial_y \\ -i\hbar\partial_x - \frac{ie}{c}Bx + \hbar\partial_y & 0 \end{bmatrix}. \tag{91}$$

The eigenvalue problem $\mathbb{H}\psi(x,y) = E\psi(x,y)$ leads to the energy values, where $\psi(x,y)$ is a spinor with two components, one for each sublattice. This problem can be solved by the separation ansatz:

$$\psi_i(x,y) = \varphi_i(y)\,\psi_i(x) = e^{(ik_y y)}\,\psi_i(x). \tag{92}$$

The problem reduces to

$$v_F \begin{bmatrix} 0 & -i\hbar\partial_x + \frac{ie}{c}Bx - i\hbar k_y \\ -i\hbar\partial_x - \frac{ie}{c}Bx + i\hbar k_y & 0 \end{bmatrix} \begin{pmatrix} \psi_1(x) \\ \psi_2(x) \end{pmatrix} = E \begin{pmatrix} \psi_1(x) \\ \psi_2(x) \end{pmatrix}. \tag{93}$$

These are two coupled differential equations. The equations can be decoupled by solving the first equation for $\psi_1(x)$

$$\psi_1(x) = -\frac{i\hbar v_F}{E}\left(\partial_x - \frac{eB}{\hbar c}x + k_y\right)\psi_2(x), \tag{94}$$

and inserting it into the second equation

$$\left(\partial_x^2 - \left(\frac{eB}{\hbar c}x - k_y\right)^2 - \frac{eB}{\hbar c}\right)\psi_2(x) = -\frac{E^2}{\hbar^2 v_F^2}\psi_2(x). \tag{95}$$

The form of this equation resembles a harmonic oscillator. To obtain the exact form, we must perform two substitutions

$$\omega = \frac{eB}{mc}, \qquad z = x - \frac{c\hbar}{eB}k_y = x - \frac{\hbar}{\omega m}. \tag{96}$$

This yields

$$\left(-\frac{\hbar^2}{2m}\partial_z^2 + \frac{1}{2}m\omega^2 z^2 + \frac{\hbar\omega}{2}\right)\psi_2(z) = \underbrace{\frac{E^2}{2mv_F^2}}_{E'}\psi_2(z). \tag{97}$$

The term $\frac{\hbar\omega}{2}$ is already diagonal and will result in an energy shift. The energy eigenvalues E' of the harmonic oscillator are

$$E'_n = \hbar\omega\,(n+1)\,. \tag{98}$$

The energy of an electron becomes

$$E_n = \pm v_F\sqrt{2m\hbar\omega(n+1)}, \tag{99}$$

and its corresponding eigenfunctions $\psi_2(x)$ are the Hermite polynomials $\varphi_n(x)$. We will substitute $n+1 \to n$, such that E_0 is equal to zero and $n \geq 0$. The corresponding eigenfunction to the energy E_n becomes φ_{n-1}. For $n = 0$ the eigenfunction $\varphi_{-1} = 0$.

Identifying the raising operator $a^\dagger$ and the lowering operator a of the harmonic oscillator, creates a different perspective for the eigenvalue problem

$$a^\dagger = \frac{1}{\sqrt{2}}\left(\sqrt{\frac{m\omega}{\hbar}}z - \sqrt{\frac{\hbar}{m\omega}}\partial_z\right), \qquad a = \frac{1}{\sqrt{2}}\left(\sqrt{\frac{m\omega}{\hbar}}z + \sqrt{\frac{\hbar}{m\omega}}\partial_z\right). \tag{100}$$

They fulfill the commutation relation

$$[a, a^\dagger] = 1, \tag{101}$$

and they are called raising operator and lowering operator because

$$a^\dagger \varphi_n(x) = \sqrt{n+1}\varphi_{n+1}(x) \qquad \text{and} \qquad a\varphi_n(x) = \sqrt{n}\varphi_{n-1}(x) \tag{102}$$

if $\varphi_n(x)$ is the solution to the eigenvalue E_n of the harmonic oscillator. The Hamiltonian $\mathbb{H}$ can also be written in terms of the raising operator $a^\dagger$ and the lowering operator a

$$\mathbb{H} = v_F\sqrt{2m\omega\hbar}\begin{bmatrix} 0 & ia^\dagger \\ -ia & 0 \end{bmatrix}. \tag{103}$$

Also $\psi_1(x)$ can be expressed by those operators ($\psi_2(x) = \varphi_n(x)$)

$$\psi_1(x) = \frac{iv_F}{E}\sqrt{2m\omega\hbar}\, a^\dagger \psi_2(x) = \pm\frac{i}{\sqrt{n+1}}\, a^\dagger \varphi_n(x) = \pm i\varphi_{n+1}(x). \tag{104}$$

The ground eigenstate ($n = 0$) of our harmonic oscillator is

$$\varphi_0 = A\exp\left(-\frac{m\omega^2}{2\hbar^2}\left(x - \frac{\hbar}{m\omega}k_y\right)^2\right). \tag{105}$$

The other eigenfunctions of the Hamiltonian are attained by acting on the ground state with the raising operator. The two-component spinor to the eigenvalue E_n now looks the following way

$$\begin{pmatrix}\psi_1(x)\\ \psi_2(x)\end{pmatrix} = \begin{pmatrix}\pm i\varphi_n(x)\\ \varphi_{n-1}(x)\end{pmatrix}. \tag{106}$$

The Hamiltonian of the other Dirac cone has almost the same form eq.(90) with a different $\vec{\alpha}' = (\sigma_1, -\sigma_2)$. Therefore the calculations are analogous to the ones above. Identifying the same raising and lowering operators as in eq.(100), leads to a Hamiltonian of the following form

$$\mathbb{H} = v_F\sqrt{2m\omega\hbar}\begin{bmatrix} 0 & -ia \\ ia^\dagger & 0 \end{bmatrix}. \tag{107}$$

The energy of an electron becomes

$$E_n = \pm v_F\sqrt{2m\hbar\omega n}, \tag{108}$$

and the eigenstates are

$$\begin{pmatrix}\psi_1(x)\\ \psi_2(x)\end{pmatrix} = \begin{pmatrix}\pm i\varphi_{n-1}(x)\\ \varphi_n(x)\end{pmatrix}. \tag{109}$$

The minus sign in the second component of $\vec{\alpha}'$ causes the energy shift $\frac{\hbar\omega}{2}$ to be added respectively subtracted in the first respectively second component of the spinor, which is exactly the other way around at the other cone.

The energy spectrum of the electrons in an external magnetic field eq.(108) is, of course, the same for both Dirac cones, but it is very interesting to notice that it is discrete because of the external magnetic field that is applied. These discrete energy values are called Landau levels. Furthermore the electron-hole symmetry still holds and there exists a state of zero energy ($n = 0$).

6 Conclusion and Outlook

In this thesis, the energy spectrum of electrons in graphene is analyzed. First, the honeycomb lattice on which the electrons propagate is investigated and the Hamiltonian of the Hubbard model, which describes the propagation of the quasi-free electrons, is introduced.

By diagonalizing the Hamiltonian, we find two symmetric energy bands due to the $SU(2)_Q$ electron-hole symmetry. However this symmetry is broken when we also consider second nearest neighbour hopping ($t' \neq 0$). The low-energy electrons are found to behave like massless relativistic particles, propagating through the honeycomb lattice with a Fermi velocity v_F, being a fraction of the speed of light. Because they have half-integer spin and a linear dispersion relation ($E(\vec{p}) = \pm v_F \left|\vec{\delta p}\right|$), they are called Dirac fermions.

An effective low-energy field theory is derived for these Dirac fermions and found to be described by the massless Dirac equation. This is in agreement with the microscopic model, which also predicts the electrons to behave like massless particles.

When an external magnetic field is applied to graphene, it changes the energy spectrum of the electrons. This is calculated using the Hubbard model, but it leads to equations only numerically solvable, which is not further pursued in this thesis. However, the energy values can be calculated analytically by the effective theory. They are quantized into energy levels called Landau levels; $E_n = \pm v_F \sqrt{2m\hbar\omega n}$. The fact that the Landau levels are calculated relatively easily by the effective low-energy field theory emphasizes its advantage over the microscopic model.

A future project is the numerical computation of the Landau levels with the Hubbard model, and afterwards, the comparison between them and the energy levels obtained from the effective theory. Furthermore, one could expand the effective theory such that it accounts for an electric field applied parallel to the graphene layer. Then one can investigate the anomalous half-integer quantum Hall effect.

Acknowledgements

I would like to thank Professor Uwe-Jens Wiese for his support and guidance. It would not have been possible to write this thesis without his expertise in this subject. I am grateful to him for always taking time for explanations and encouraging me.

My thanks go also to my fellow students Stephan Caspar and Sacha Schwarz with whom I had many enlightening discussions, which helped me to advance when I got stuck and to better understand the topic.

References

[1] A.K. Geim. Graphene: Status and Prospects. *Science*, 324:1530, (2009).

[2] A.H. Castro Neto, F. Guinea, N.M.R. Peres, K.S. Novoselov, and A.K. Geim. The Electronic Properties of Graphene. *Rev. Mod. Phys.*, 81:109, (2009).

[3] *http* : *//commons.wikimedia.org/wiki/File* : *Graphenegraphite_relation.png?uselang* = *de*, 14. July (2011).

[4] J. Balmer. Festkörperphysik. Lecture Notes, University of Bern, Chapter 1 and 2, (2010).

[5] B. Bessire. Spiral phases from a Systematic Low-Energy Effective Field Theory for Magnons and Holes in an Antiferromagnet on the Honeycomb Lattice. Master's thesis, University of Bern, *http* : *//www.wiese.itp.unibe.ch/theses/bessire_master.pdf*, (2009).

[6] C.N. Yang and S.C. Zhang. SO(4) Symmetry in the Hubbard Model. *Mod. Phys. Lett.*, B4:759, (1990).

[7] J. Fröhlich and U.M. Studer. Gauge Invariance and Current Algebra in Nonrelativistic Many-body Theory. *Mod. Phys.*, 65:733, (1995).

[8] E.V. Castro, N.M.R. Peres, J.M.B. Lopes dos Santos, F. Guinea, A.H. Castro Neto, V. Rocha Vieira, P.D. Sacramento, and J.M.P. Carmelo. *Strongly Correlated Systems, Coherence and Entanglements*. World Scientific Publishing Co. Pte. Ltd., (2007). Chapter 4: An Introduction to the Physics of Graphene Layers.

[9] F. Kämpfer, M. Moser, and U.-J. Wiese. Systematic Low-Energy Effective Theory for Magnons and Charge Carriers in an Antiferromagnet. *Nucl. Phys.*, B729:317, (2005).

[10] M. Mecklenburg and B.C. Regan. Spin and the Honeycomb Lattice: Lessons from Graphene. *Phys. Rev. Lett.*, 106:116803, (2011).

[11] A.A. Kozhevnikov. Tight Binding and Emergence of "Dirac" equation in Graphene. *http* : *//www.inp.nsk.su/chairs/theor/postgraduate_courses/Kozhevnikov.pdf*, Presentation, (2010).

[12] U.-J. Wiese. Quantum Mechanics. *http* : *//www.wiese.itp.unibe.ch/lectures/quantum.pdf*, Lecture Notes, University of Bern, Chapter 6, (2010).

[13] U.-J. Wiese. Statistical Mechanics. *http* : *//www.wiese.itp.unibe.ch/lectures/thermodyn.pdf*, Lecture Notes, University of Bern, Chapter 15, (2010).